Reconstitution of Native-type Noncrystalline Lens Fiber Gap Junctions from Isolated Hemichannels

Joerg Kistler,* Kenneth Goldie,‡ Paul Donaldson,* and Andreas Engel‡

*School of Biological Sciences, Center for Gene Technology, University of Auckland, Auckland, New Zealand; and ‡M. E. Müller Institute for Microscopic Structural Biology, Biozentrum, University of Basel, Basel 4056, Switzerland

Abstract. Gap junctions contain numerous channels that are clustered in apposed membrane patches of adjacent cells. These cell-to-cell channels are formed by pairing of two hemichannels or connexons, and are also referred to as connexon pairs. We have investigated various detergents for their ability to separately solubilize hemichannels or connexon pairs from isolated ovine lens fiber membranes. The solubilized preparations were reconstituted with lipids with the aim to reassemble native-type gap junctions and to provide a model system for the characterization of the molecular interactions involved in this process. While small gap junction structures were obtained under a variety of conditions, large native-type gap junctions were assembled using a novel two-step procedure: in the first step, hemichannels that had been solubilized with octylpolyoxyethylene formed connexon pairs by dialysis against n-decyl-beta-D-maltopyranoside. In the second step, connexon pairs were reconstituted with phosphatidylcholines by dialysis against buffer containing Mg^{2+}. This way, double-layered gap junctions with diameter $\leqslant$ 300 nm were obtained. Up to several hundred channels were packed in a noncrystalline arrangement, giving these reconstituted gap junctions an appearance that was indistinguishable from that of the gap junctions in the lens fiber membranes.

ONNEXINS are a family of proteins that form cell-to-cell channels often found clustered in the form of gap junctions. The cell-to-cell channels are connexon pairs that are formed by the pairing of two single connexons or hemichannels. Sequences for numerous connexins have been established (Kumar and Gilula, 1992; Bennett et al., 1991; Willecke et al., 1991; Beyer et al. 1990). Using molecular probes based on this sequence information, it has become possible to study the dynamic connexin expression patterns during tissue differentiation (Kren et al., 1993; Risek et al., 1992; Yancey et al., 1992; Nishi et al., 1991). Expression of specific connexins in heterologous systems in combination with electrophysiology has greatly advanced our understanding of the functional properties of cell-to-cell channels (Fishman et al., 1990; Swenson et al., 1989). In contrast to these areas of rapid progress, we have relatively little knowledge about the gap junction assembly process. Considering the rapid turnover rates of gap junctions in vivo (Fallon and Goodenough, 1981; Laird et al., 1991), it is important to characterize the molecular interactions driving gap junction assembly as these are undoubtedly relevant for the regulation of intercellular communication.

The relatively delayed research of gap junction assembly is probably related to the fact that the biochemical characterization of gap junction proteins has been limited to only a few cell systems, notably liver (connexin26 and connexin32; Hertzberg, 1984; Nicholson et al., 1987; Stauffer et al., 1991; Paul, 1986; Kumar and Gilula, 1986; Zhang and Nicholson, 1989), heart (connexin 43; Manjunath et al., 1985; Yeager and Gilula, 1992; Beyer et al., 1987), and lens (connexin46 and connexin50; Kistler et al., 1988, 1990a; Paul et al., 1991; White et al., 1992). Most other connexins are only known by sequence but have never been isolated as protein. Two different experimental avenues have been used to study the molecular interactions involved in gap junction assembly. In one, the intracellular synthesis and oligomerization of connexins was investigated (Revel et al., 1992). For connexin43, hemichannels were found to form in the *trans*-Golgi network (Musil and Goodenough, 1993). Further assembly to gap junctions appeared to be dependent on the state of connexin phosphorylation and the presence of adhesion proteins in the plasma membrane (Musil et al., 1990; Musil and Goodenough, 1991). Alternatively, an in vitro system was developed for the assembly of gap junctions from detergent-solubilized channel structures and lipids from lens fiber cells (Lampe et al., 1991). These reconstituted gap junctions were large and had channels in a crystalline arrangement. Cleavage of lens gap junction protein (connexin46 and connexin50) and the presence of Mg^{2+} were necessary prerequisites, suggesting that protein–protein interactions were a major driving force for crystalline gap junction formation in vitro. This was in stark contrast with the situation in the lens fiber membranes: gap junctions assembled in vivo have uncleaved connexin and are non-

Address correspondence to Andreas Engel, MSB Biozentrum, University of Basel, Klingelbergstrasse 70, 4056 Basel, Switzerland.

crystalline (Kuszak et al., 1982; Zampighi et al., 1989; Kistler et al., 1990a; Lo and Reese, 1993). Attempts to reconstitute native-type noncrystalline gap junctions from uncleaved protein were only partially successful: they were limited to an average size of 25–40 nm and contained only ∼10 channels (Kistler et al., 1993).

We now report on the development of a novel procedure for the assembly of native-type lens fiber gap junctions in vitro that starts from hemichannels and uses defined lipid mixtures for reconstitution. Formation of connexon pairs from hemichannels and lateral assembly of the latter were accomplished in two separate steps. This way, noncrystalline gap junctions comprising several hundred channels were produced, and they were indistinguishable from those assembled in the lens fiber membranes in vivo.

Materials and Methods

Isolation of Lens Fiber Membranes

Membranes were isolated from sheep lens outer cortex. Typically, ∼100 lenses were processed together. Lenses were decapsulated and outer cortex tissue was dissected and pooled. All procedures were carried out at 4°C unless stated otherwise. Outer cortex tissue was homogenized in 300 ml 5 mM Tris-HCl, pH 8.0, 5 mM EDTA, and 5 mM EGTA. Crude membranes were pelleted at 11,000 rpm for 20 min Sorvall SS-34) and washed twice in the same buffer. Proteins adhering to the membranes were removed by solubilization in 100 ml 4 M urea, 5 mM Tris-HCl, pH 9.5, 5 mM EDTA, 5 mM EGTA, and centrifugation at 40,000 rpm for 40 min (TFT 70.38; Kontron Electronics, Inc., Redwood City, CA). Membranes were further extracted twice with 100 ml 20 mM NaOH and subsequently washed once in 100 ml 5 mM Tris-HCl, pH 8.0, 2 mM EDTA, 2 mM EGTA, and 100 mM NaCl. These urea/alkali stripped membranes were resuspended at a protein concentration of ∼6 mg/ml and stored frozen at −70°C. Protein concentrations were determined using the Lowry procedure (Lowry et al., 1951) adapted to membrane proteins by inclusion of 1% butanol in the reagent solutions.

Solubilization of Channel Structures and Sucrose Gradient Analysis

Channel structures (hemichannels or connexon pairs) were solubilized with detergent under low salt conditions. Urea/alkali-stripped membranes were washed twice in 10 mM Hepes, pH 7.2, before adding detergent to final concentrations of either 2% octyl-beta-D-glucopyranoside (8-GLU)[1] (Bachem, Bubendorf, Switzerland), 0.5% n-decyl-beta-D-maltopyranoside (10-MALT) (Sigma Chemical Co., St. Louis, MO), or 1% octylpolyoxyethylene (8-POE) (Bachem). The total protein concentration in the solubilization mixture was 3 mg/ml. After 5 min at 23°C, unsolubilized material was pelleted at 40,000 rpm for 40 min (TLA-100.2; Beckman Instruments Inc., Fullerton, CA). The proportion of hemichannels and connexon pairs in the soluble fraction was determined by separation on 5–20% sucrose gradients and detection of gradient peaks by dot blot analysis with anti-MP70 and radioactive secondary antibodies (Kistler et al., 1993). Anti-MP70 antibodies (Kistler et al., 1985) label lens fiber connexin50 (White et al., 1992). SDS-PAGE of detergent-soluble and -insoluble proteins, as well as gradient fractions, was carried out according to Laemmli (1970).

Formation of Connexon Pairs from Hemichannels

Preparations enriched in hemichannels were obtained by selectively solubilizing gap junctions from urea/alkali stripped membranes with 8-POE. Hemichannels formed connexon pairs by dialyzing 700-μl aliquots of

---

1. *Abbreviations used in this paper*: CMC, critical micelle concentration; CTEM, conventional transmission electron microscopy; DMPC, L-beta-gamma-dimyristoyl phosphatidylcholine; DPPE, L-beta-gamma dipalmitoyl phosphatidylethanolamine; 8-GLU, octyl-beta-D-glucopyranoside; LPR, lipid/protein ratio; 10-MALT, n-decyl-beta-D-maltopyranoside; MPA, mass per area; OPPC, L-beta palmitoyl-gamma oleoyl phosphatidylcholine; 8-POE, octylpolyoxyethylene; STEM, scanning transmission electron microscopy.

8-POE–solubilized material against 400 ml 0.25% 10-MALT, 10 mM Hepes, pH 7.2, and 0.005% NaN₃ for 48 h at 4°C.

Crude Assembly Protocol

Gap junction structures were reconstituted from solubilized mixtures containing hemichannels or connexon pairs and endogenous lipids (Lampe et al., 1991). For this, 100-μl aliquots of solubilized material were dialyzed against 1 liter 10 mM Hepes, pH 7.2, 20 mM MgCl₂, and 0.005% NaN₃ for 72 h at 23°C. The dialysis buffer was renewed once after 24 h.

Gradient Assembly Protocol

Gap junction structures were reconstituted from sucrose gradient–isolated hemichannels or connexon pairs and solubilized lipids of defined concentrations and combinations. 50-μl aliquots of gradient fractions with a protein concentration of 0.2 mg/ml were mixed with an equal volume of lipids that had been solubilized at a concentration of 0.2 mg/ml with the same detergent as that contained in the gradient. This lipid/protein ratio (LPR) of 1 was used unless stated otherwise. Lipids (Sigma Chemical Co.) were used alone or in combinations and were: L-beta-gamma dimyristoyl phosphatidylcholine (DMPC), L-beta palmitoyl gamma oleoyl phosphatidylcholine (OPPC), L-beta-gamma dipalmitoyl phosphatidylethanolamine (DPPE), sphingomyelin. Protein-lipid mixtures were dialyzed against 1 liter 10 mM Hepes, pH 7.2, 20 mM MgCl₂, and 0.005% NaN₃ for 72 h at 23°C. The dialysis buffer was renewed once after 24 h.

Conventional Transmission Electron Microscopy (CTEM)

Sucrose gradient–isolated hemichannels or connexon pairs, or reconstituted membranes, were viewed by negative-stain electron microscopy. They were adsorbed to freshly glow discharged carbon/collodion coated grids and negatively stained with 2% uranyl acetate. Specimens were examined with an electron microscope (H8000; Hitachi Instruments, Inc., San Jose, CA) operated at 100 kV, and micrographs were recorded at a magnification of 40,000 on electron image film (SO-163; Eastman Kodak, Rochester, NY) at a dose of typically 2,000 electrons/nm².

Scanning Transmission Electron Microscopy (STEM) and Mass Analysis

STEM mass analysis (Engel and Colliex, 1993) was carried out for solubilized hemichannels, connexon pairs, reconstituted mini gap junctions, and gap junction sheets. Samples were adsorbed to glow discharged thin carbon films supported by fenestrated films, and they were extensively washed in double-distilled water. The specimens were quick frozen in liquid nitrogen and freeze dried at −80°C and a pressure of 10⁻⁸ Torr in a pretreatment chamber that was directly connected to a Vacuum Generators HB5 STEM. Elastic dark-field images were recorded at 80 kV acceleration voltage and doses between 290 and 440 electrons/nm². Digital acquisition of the microscope parameters and image data, system calibration, and mass analysis were carried out as previously described (Müller et al., 1992). This procedure was applicable without modifications to solubilized channel structures and gap junction sheets, but a different method was used for the mass analysis of the mini gap junctions. For the latter, the mass of each of 54 well-preserved mini gap junctions was determined by integrating the elastically scattered electrons within a contour larger than the mini gap junction. The function "analyze" of the SEMPER image processing system (Saxton et al., 1979) was used to determine the area of each gap junction. Mass per area (MPA) values were then calculated for each mini gap junction and plotted as a histogram.

To determine the average area occupied by a channel structure, dark-field images of uranyl acetate–stained mini gap junctions were recorded at 100 kV and doses in the range of 3,000–4,000 electrons/nm². The high contrast and clearness of these images allowed channels to be counted unambiguously for each mini gap junction. The area of each mini gap junction was calculated using an ellipse-fitting function. Plots of area vs number of channels and linear regressions were produced with the program Cricket Graph installed on a Macintosh computer.

Results

Solubilization of Hemichannels and Connexon Pairs

Urea/alkali-stripped fiber membranes of the lens outer cor-

tex contain as major integral proteins MIP26, MP20, and the gap junction polypeptides connexin46 and connexin50. In ovine lens fiber membranes, these connexins comigrate as a 70/64-kD doublet by SDS-PAGE (Kistler et al., 1988; White et al., 1992). The connexin topology in urea/alkali-stripped membranes appeared to be unaltered from native membranes using immunogold labeling (Kistler and Bullivant, 1988), limited proteolysis (Kistler et al., 1990b), or electrophysiology (Donaldson and Kistler, 1992) as criteria. Detergents with moderately high critical micelle concentration (CMC) values suitable for reconstitution experiments were screened for their solubilization profile of the lens outer cortex fiber membrane proteins. We routinely used detergents at two to six times CMC in 10 mM Hepes, pH 7.2, and at room temperature. 2% 8-GLU (CMC = 0.89%, 30 mM), 0.5% 10-MALT (CMC = 0.08%, 1.6 mM), and 1% 8-POE (CMC = 0.23%, 6 mM) effectively solubilized all connexin (Fig. 1, b–g). They differed, however, in the amounts solubilized of the other membrane proteins. Most importantly, 8-POE showed some degree of selectivity for connexin because this detergent solubilized significantly less MIP26 and MP20 compared to 8-GLU or 10-MALT (Fig. 1, f and g). A protein fraction obtained by solubilization with 8-GLU of membranes pre-extracted with 8-POE, containing MIP26 and MP20 but was totally deficient of connexin (Fig. 1, h and i). A similar degree of selectivity for connexin solubilization had previously been found for TX-100 (Kistler and Bullivant, 1988), but this detergent was not used here because its relatively low CMC (0.02%, 0.24 mM) rendered it unsuitable for the reconstitution experiments. The selectivity of 8-POE for connexin solubilization had the great advantage of a major single step enrichment of channel structures.

Detergent solubilization of lens fiber gap junctions had previously been shown to generate both hemichannels and connexon pairs (Kistler et al., 1993). Sedimentation analysis had been used to assay the proportion of hemichannels and connexon pairs in the soluble fraction. For this, solubilized channel structures had been separated on a 5–20% sucrose gradient and detected by immunodotblotting the gradient
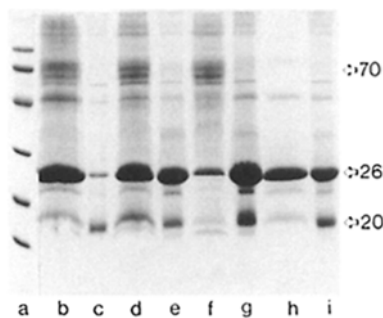

Figure 1. Solubilization of lens fiber membrane proteins with detergents. SDS-PAGE (12% acrylamide) of detergent soluble and insoluble fractions. (*a*) Molecular weight markers from top, × 1,000; 97, 66, 43, 31, 22, and 14; (*b*) 8-GLU–soluble fraction; (*c*) 8-GLU–insoluble fraction; (*d*) 10-MALT–soluble fraction; (*e*) 10-MALT–insoluble fraction; (*f*) 8-POE–soluble fraction; (*g*) 8-POE–insoluble fraction; (*h*) 8-GLU–soluble fraction of membranes pre-extracted with 8-POE; (*i*) 8-GLU–insoluble fraction of membranes pre-extracted with 8-POE.

fractions with anti-MP70 and radioactive secondary antibodies. Negative-stain electron microscopy had shown that the gradient peak containing 9S particles was enriched in doughnut-shaped structures consistent with hemichannels, whereas the 16S peak was enriched in dumbbell-shaped structures consistent with connexon pairs. Using the same assay, we now show that both 8-GLU– and 10-MALT–solubilized channel structures are predominantly in the 16S form, i.e., connexon pairs (Fig. 2 *a*). In contrast, channel structures solubilized with 8-POE sedimented mostly as 9S hemichannels. 8-MALT produced both hemichannels and connexon pairs (data not shown).

The identification by negative-stain electron microscopy of 9S and 16S particles as hemichannels and connexon pairs, respectively, was double-checked with STEM mass analysis of freeze-dried unstained channel structures that had been isolated from the gradient peaks (Engel and Colliex, 1993). 9S and 16S particles had average masses of 388 ± 52 kD (n = 303) and 724 ± 118 kD (n = 100), respectively (Fig. 2, *b* and *c*). These values are in good agreement with the ∼300- and 600-kD masses expected for the hexameric connexin46/50 hemichannels and dodecameric connexon pairs (Paul et al., 1991; White et al., 1992). The widths of the Gaussian peaks fitted to the mass histograms are likely to reflect some variability of detergent binding and carbon film variations.

Taken together, these results show that it is not possible to predict on the basis of the type of headgroup or the length of the alkyl chain whether a detergent solubilizes connexin as hemichannels or connexon pairs. 8-GLU, 8-MALT, and 8-POE all have C8 chains, yet they produced different proportions of hemichannels and connexon pairs. Different solubilization products were also obtained with 8-POE and TX-100, which have a common polyoxyethylene head group and exhibit a similar degree of selectivity for connexin46/50: the former produced hemichannels, whereas the latter had previously been shown to produce predominantly connexon pairs (Kistler et al., 1993). Importantly, however, the different solubilization profiles of detergents can be exploited to our advantage in that they can be used to produce separately hemichannels or connexon pairs.

Formation of Connexon Pairs

If hemichannels are stable in 8-POE, and the detergents 8-GLU and 10-MALT favor connexon pairs, it could be predicted that exchange of 8-POE with 8-GLU or 10-MALT by dialysis might result in the formation of connexon pairs from hemichannels. A concomitant shift of the gradient peak from 9S to 16S would be expected. Indeed, this was the case: detergent exchange by dialysis during 3 d at 4°C led to a reduction of the 9S peak and the appearance of a new peak at the 16S position in the gradient (Fig. 2 *d*). This shift was more pronounced for material dialyzed against 10-MALT than for 8-GLU.

A preliminary characterization of the type of molecular interactions involved in connexon pairing was aimed at detecting the potential involvement of disulfide groups (each connexin subunit contains six cysteines in its extracellular peptide segments) or ionic interactions. For this, the dialysis solution contained, in addition to 0.25% 10-MALT, 10 mM Hepes, pH 7.2, either 5 mM DTT or 500 mM NaCl, 5 mM EDTA, 5 mM EGTA, and 5 mM DTT. Neither of these addi-
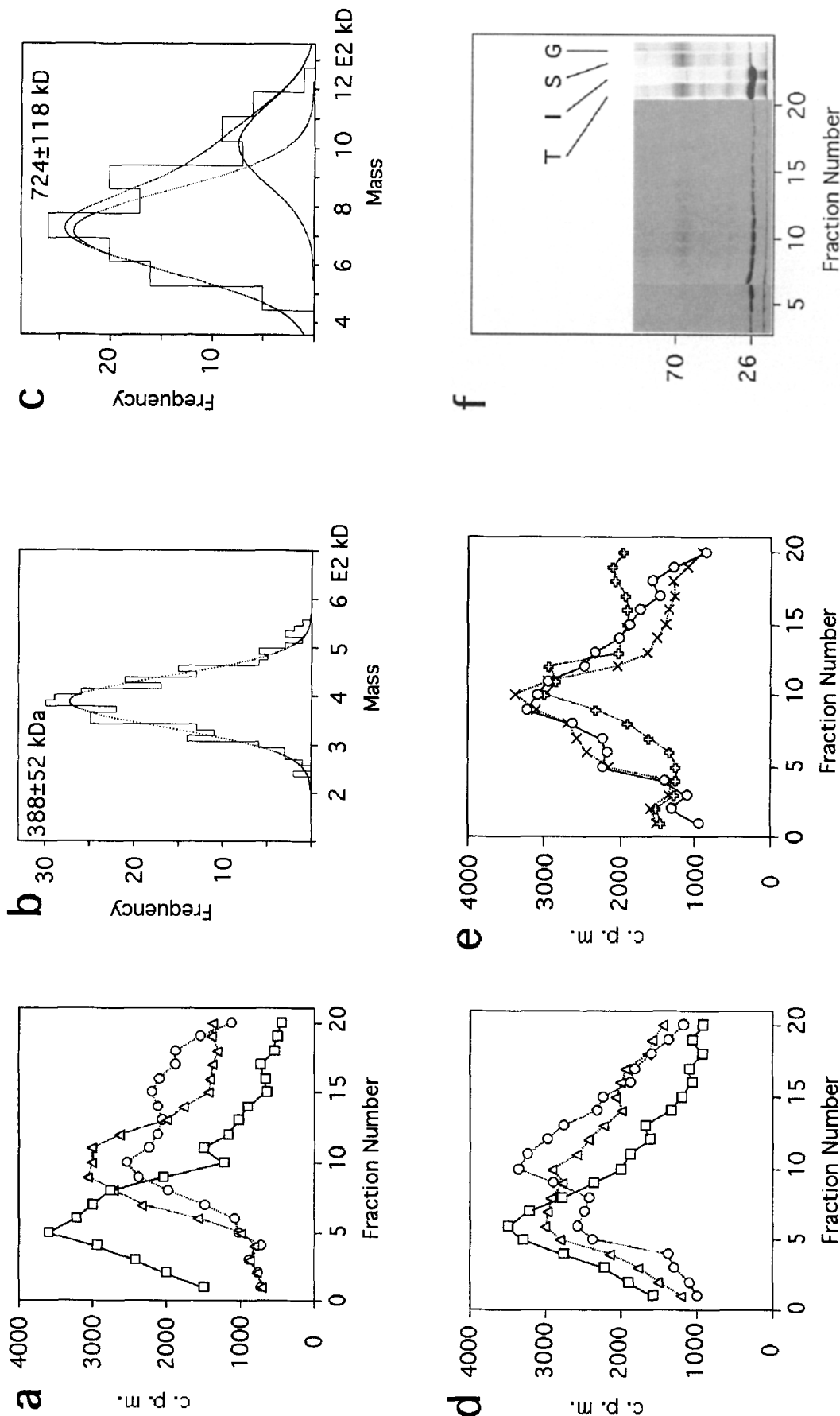
Figure 2. Solubilization of hemichannels and connexon pairs and pairing of hemichannels. (*a*) Sedimentation analysis. Graph shows levels of connexin detected with anti-MP70 and radioactive secondary antibodies as cpm for each gradient fraction. Hemichannels (fraction 5/6) and connexon pairs (fraction 10) have sedimentation values of 9S and 16S, respectively. Membranes were solubilized with 8-GLU (*triangles*), 10-MALT (*circles*), or 8-POE (*squares*). (*b* and *c*) STEM mass analysis. Mass peaks are (*b*) 388 ± 52 kD (*n* = 303) for hemichannels and (*c*) 724 ± 118 kD (*n* = 100) for connexon pairs (major Gaussian peak). In agreement with the sedimentation analysis shown in *a* for 10-MALT (*circles*), a small fraction of larger connexon aggregates was also observed (minor Gaussian peak). (*d*) Sedimentation analysis: Formation of connexon pairs by dialysis of 8-POE solubilized hemichannels (*squares*) against 8-GLU (*triangles*) or 10-MALT (*circles*). (*e*) Sedimentation analysis: Formation of connexon pairs by dialysis of 8-POE solubilized hemichannels against 10-MALT (*circles*) or 10-MALT/DTT (*X's*) or 10-MALT/DTT/NaCl/EDTA/EGTA (*crosses*). (*f*) SDS-PAGE. Minigel (10% acrylamide) showing protein profile in gradient of 8-GLU solubilized fiber membrane proteins. Gel lanes *T-G* document enrichment of connexin70 by 8-POE solubilization and gradient sedimentation. *T*, total lens fiber membrane protein; *I*, 8-POE-insoluble protein; *S*, 8-POE-soluble protein; *G*, gradient-isolated hemichannels.

tions prevented the shift of the gradient peak from 9S to 16S (Fig. 2 *e*). Hence, ionic interactions and disulfide bonds appear unlikely to play a major role in connexon pairing.

Protein Analysis of Gradients

Our gradient system was an effective tool for separating solubilized hemichannels and connexon pairs. We further analyzed the protein profile in the gradients with SDS-PAGE to see whether separation of connexins and nonconnexin proteins was also achieved. Of particular interest was the sedimentation behavior of MIP26, which had previously been the subject of some controversy regarding whether this polypeptide was a component of the lens fiber gap junction (Paul and Goodenough, 1983; Sas et al., 1985). The distribution of MIP26 in the gradient was best visualized using 8-GLU–solubilized material because this detergent solubilized more of this membrane polypeptide than the other detergents tested. MIP26 peaked in gradient fraction 6 but spread throughout the gradient (Fig. 2 *f*). As result of this, some enrichment of connexin (peak in fraction 10), but not complete separation from MIP26, was achieved in this case. The best enrichment of connexin was obtained by the use of 8-POE–solubilized material, as also shown in Fig. 2 *f*: all connexin contained in the total membrane (T) was solubilized (S), whereas most MIP26 was insoluble (I). After gradient separation (G), small amounts of MIP26 were still present, but connexin was the predominant protein. Hence, direct interactions between MIP26 and connexin appear unlikely, but cannot entirely be ruled out.

In summary, while further enrichment of connexin was achieved, the main advantage of using the gradients was their effectiveness in producing channel preparations that were defined in terms of their content of hemichannels and connexon pairs.

Assembly of Gap Junction Structures from Connexon Pairs

In pursuit of the aim to reconstitute large native-type noncrystalline gap junctions similar to those in the lens fiber membranes, we first tested the hypothesis that starting out from connexon pairs instead of hemichannels would be more efficient and result in larger structures. Only lateral assembly of connexon pairs and lipid molecules would appear to be needed to produce gap junctions in vitro. Connexon pairs solubilized either with 8-GLU or with 10-MALT were used for these reconstitution experiments. Two distinct reconstitution protocols were used. In the first procedure, which we refer to as "crude assembly" and which had previously been introduced (Lampe et al., 1991), detergent was removed from solubilized mixtures of channel structures, nonjunctional proteins, and endogenous lipids by dialysis against large quantities of buffer. A portion of these solubilized mixtures was analyzed by sucrose gradient sedimentation to verify that the channel structures were present predominantly as connexon pairs. Alternatively, in the second procedure, referred to as "gradient assembly," connexon pairs were isolated from gradients and mixed with various solubilized, defined mixtures of lipids. Detergent was subsequently removed by dialysis. In both procedures, reconstituted samples were analyzed by negative-stain electron microscopy for evidence of gap junction assembly. Gap junction structures could be identified either as clusters of channels when viewed face-on, or as double membrane structures when viewed side-on.

Crude assembly using 8-GLU–solubilized lens outer cortex fiber membrane proteins and lipids produced small gap junctions or "mini gap junctions," as well as larger sized amorphous membrane vesicles and sheets (Fig. 3 *a*). In control experiments, using membranes from which connexin had been extracted with 8-POE and which contained predominantly MIP26 as starting material, (Fig. 1 *h*), only the amorphous membrane vesicles and sheets were obtained (Fig. 3 *b*). This result validates the identification of mini gap junctions as assembly product of connexin, in agreement with previous immunolabeling data (Kistler et al., 1993). While the mini gap junctions shown in this report were obtained with preparations containing channel structures exclusively as connexon pairs, they were indistinguishable in aspect and size from those previously obtained with ~1:1 mixtures of hemichannels and connexon pairs (Kistler et al., 1993). In both cases, mini gap junctions were mostly 25–40 nm in diameter and had an upper size limit of ~100 nm. Similar results were also obtained using 10-MALT–solubilized connexon pairs for crude assembly (data not shown). Hence, assembly from exclusively connexon pairs in the crude assembly mixture did not produce larger gap junction structures than previously obtained.

For the gradient assembly procedure, 8-GLU–solubilized connexon pairs were isolated from the sucrose gradient and mixed with 8-GLU–solubilized lipids in different combinations before removal of the detergent by dialysis. A protein concentration of 0.1 mg/ml and LPR = 1 was generally maintained. In all cases, however, connexon pairs aggregated and only amorphous membrane vesicles or sheets were formed without any sign of incorporation of channels (data not shown). Prolonged exposure to 8-GLU apparently led to denaturation and aggregation of connexon pairs and rendered them incapable for gap junction assembly. This result was not unexpected from previous experiments that had shown that the assembly of hexagonal lattices from cleaved connexin was similarly sensitive to prolonged exposure to 8-GLU (Lampe et al., 1991). In contrast, 10-MALT–solubilized connexon pairs isolated from gradients were successfully incorporated into lipid bilayers, and they formed small gap junctions. These were recognized as small clusters of channels integrated in larger membrane vesicles (Fig. 3, *c–f*). They were similar in size to the mini gap junctions described above, but were different from the latter in that they were not independent but often integrated into larger membranes. The structures shown were obtained with a 1:1 mixture of DMPC and OPPC and LPR = 1. The protein concentration was maintained at 0.1 mg/ml. Generally similar results, with some size variability of reconstituted membranes and gap junctions, were obtained with a wide range of combinations of these lipids. We never detected channels individually positioned in the membranes but always found them clustered.

By starting assembly from connexon pairs, we predicted that the reconstituted gap junctions were likely to be double layered, as evidenced by double-membrane structures seen as side views. However, face-on views could theoretically represent either single- or double-layered structures. This uncertainty was resolved using STEM mass measurement of unstained, freeze-dried gap junctions (Engel and Colliex, 1993). Because low-dose elastic STEM dark-field images of
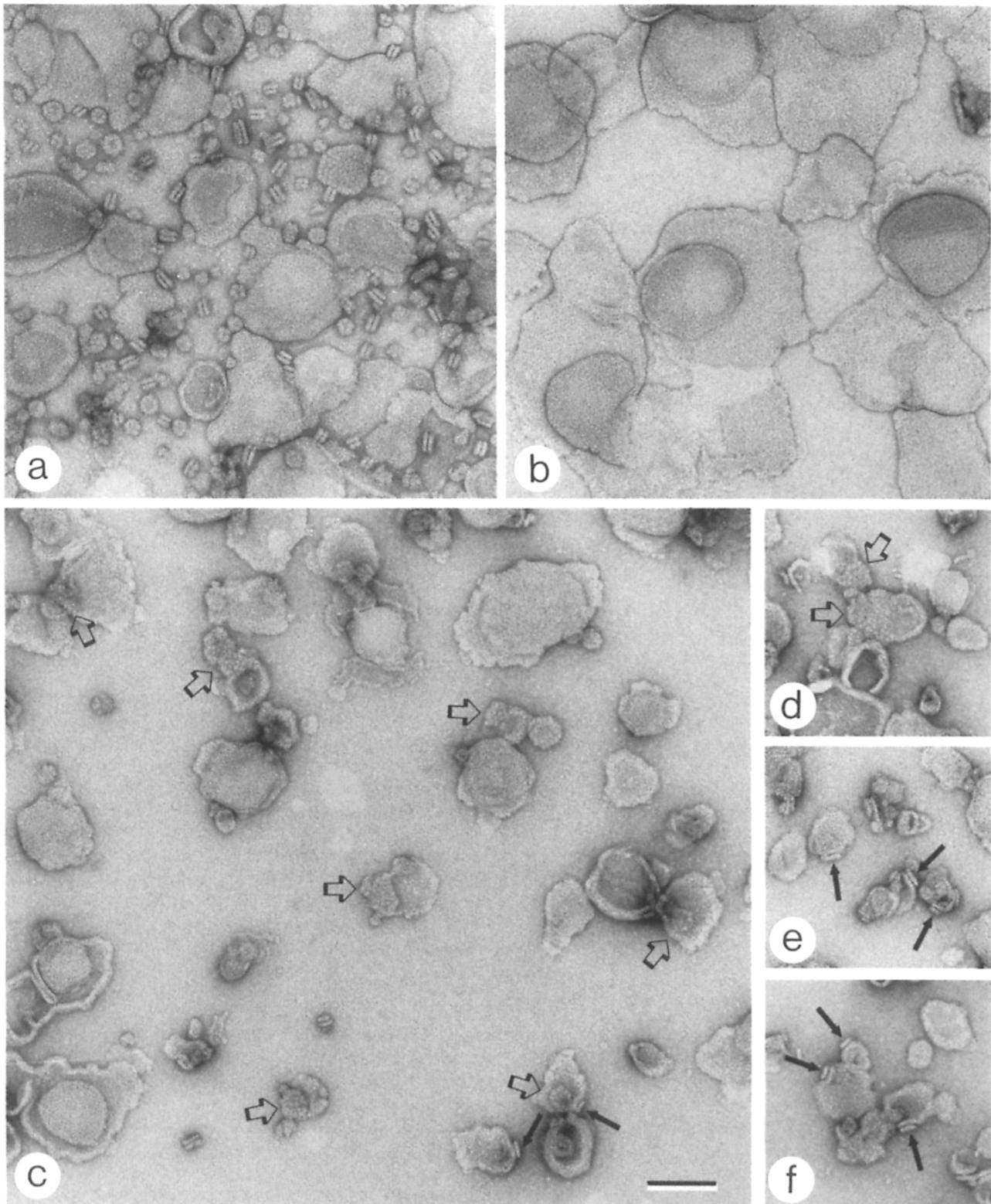
Figure 3. Assembly of gap junction structures from connexon pairs. (*a*) Crude assembly protocol. Assembly of mini gap junctions and membranes from 8-GLU–solubilized lens fiber membrane proteins and lipids. Mini gap junctions are seen as double-layered side views or as channel clusters in face-on views. (*b*) Same procedure as in *a*, except 8-POE preextracted fiber membranes were used for solubilization with 8-GLU. Note the absence of mini gap junctions. (*c–f*) Gradient assembly protocol. (*c*) Overview and (*d–f*) individual views of gap junction structures reconstituted from 10-MALT solubilized connexon pairs and DMPC/OPPC at LPR = 1. Gap junctions are mostly integrated in larger membranes and seen as clusters of channels (*thick arrows*) or short double-layered structures (*thin arrows*). Bar, 100 nm.
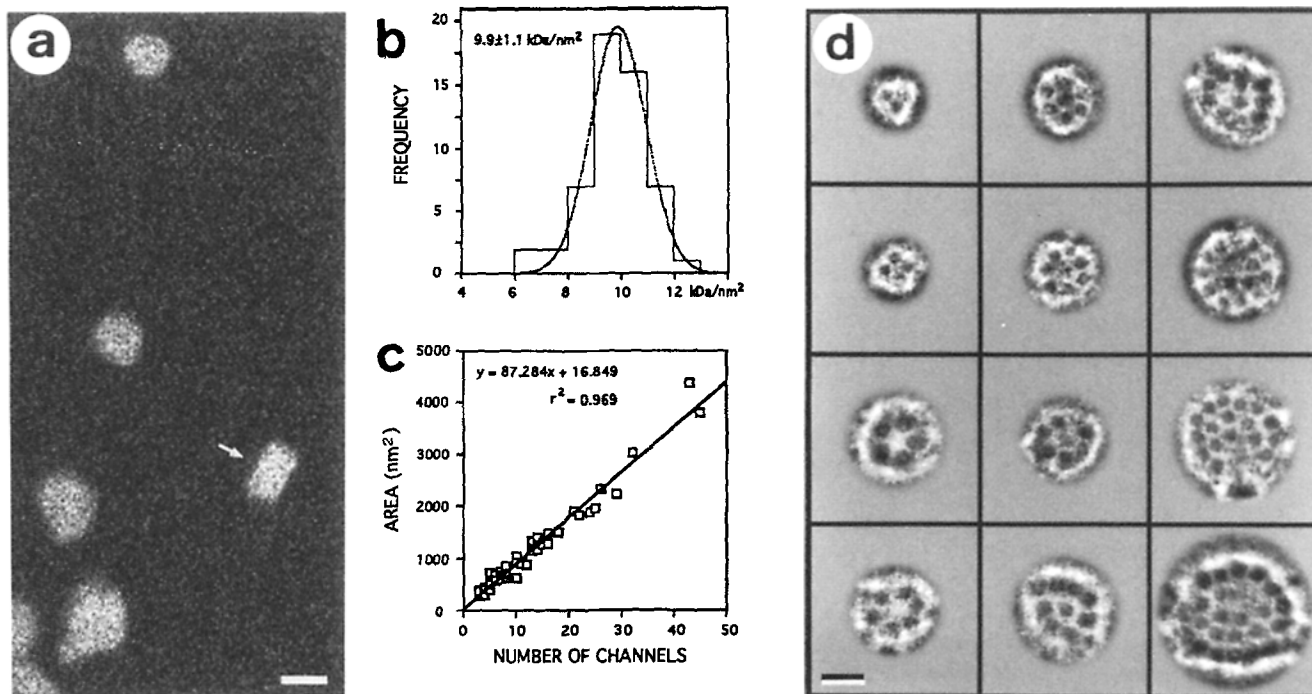
Figure 4. STEM mass analysis of mini gap junctions. (a) STEM dark-field image of freeze-dried unstained mini gap junctions recognized as near circular shapes (face-on view) or rectangular shapes (side view, *arrow*). (b) MPA calculated for each mini gap junction and plotted as a histogram. The MPA peak is at 9.9 ± 1.1 kD/nm². (c) Number of channel structures plotted against area of mini gap junctions, yielding an average value for the bilayer area occupied by each channel structure of 87.3 nm². (d) Gallery of negatively stained mini gap junction face-on views imaged with STEM dark field. The channel structures are seen with high contrast and can be easily counted for each gap junction. Bars, 20 nm in *a* and *d*.

these gap junctions did not reveal channels typically seen in negatively stained gap junctions, mass measurements were only applicable to the mini gap junctions that could be identified on the basis of their distinct shapes and dimensions: face-on views were patches of 20–50 nm diameter, while side views exhibited a rectangular outline (Fig. 4 *a*). Face-on views of well-preserved mini gap junctions were selected and their MPA values were determined (Fig. 4 *b*). To interpret the MPA peak at 9.9 ± 1.1 kD/nm², the average number of channels per area was measured from STEM dark-field images of negatively stained mini gap junctions (Fig. 4 *d*). Fig. 4 *c* illustrates that the number of channels increased linearly with the gap junction area, yielding for the average bilayer area each channel structure occupied a value of 87.3 nm². Using this value, a cross-section of 34 nm²/channel, a mass of the connexin46/50 dodecameric connexon pair of 600 kD (Paul et al., 1991; White et al., 1992), and a lipid bilayer MPA of 2.6 kD/nm² (Lampe et al., 1991), the MPA of double-layered mini gap junctions was estimated to be 10 kD/nm². This value is in excellent agreement with that measured above, proving that assembly with exclusively connexon pairs consistently produced double-layered mini gap junctions.

In summary, both crude and gradient assembly procedures demonstrate the ability of the connexon pairs to spontaneously assemble laterally and form gap junction structures. Dependent on the procedure and detergent, these in vitro-assembled gap junctions can have the form of mini gap junctions, which are independent of other membranes, or they can be integrated into larger membranes. In the case of the

mini gap junctions, we have been able to verify that they are all double layered. In both cases, however, the assembly from exclusively connexon pairs did not produce larger gap junctions than those previously obtained (Kistler et al., 1993).

Gap Junction Assembly Starting from Hemichannels

Two reactions, connexon pairing and lateral assembly, are needed to assemble gap junctions from hemichannels and lipids. Only 8-POE–solubilized channel structures could be used for these reconstitution experiments because only this detergent produced a single 9S gradient peak. 8-POE–solubilized preparations further had the advantage of a greater enrichment of connexin than was achieved with the other detergents. Doughnut-shaped hemichannels and no dumbbell-shaped structures (connexon pairs) were observed by negative-stain electron microscopy of 8-POE solubilized-channel structures (Fig. 5 *a*). Crude assembly produced small membrane patches that were likely to be single-layered based on the total absence of double-layered side views (Fig. 5 *b*). The membrane patches contained integrated protein structures that often had the appearance of channels, albeit with lower contrast compared to those found in double-layered gap junctions. This failure to produce double-layered gap junction structures led to the development of a two-step assembly procedure with separate steps for connexon pairing and lateral assembly. As the first step, 8-POE, which was used for the initial solubilization of hemichannels, was exchanged with 10-MALT, thus allowing hemichannels to com-
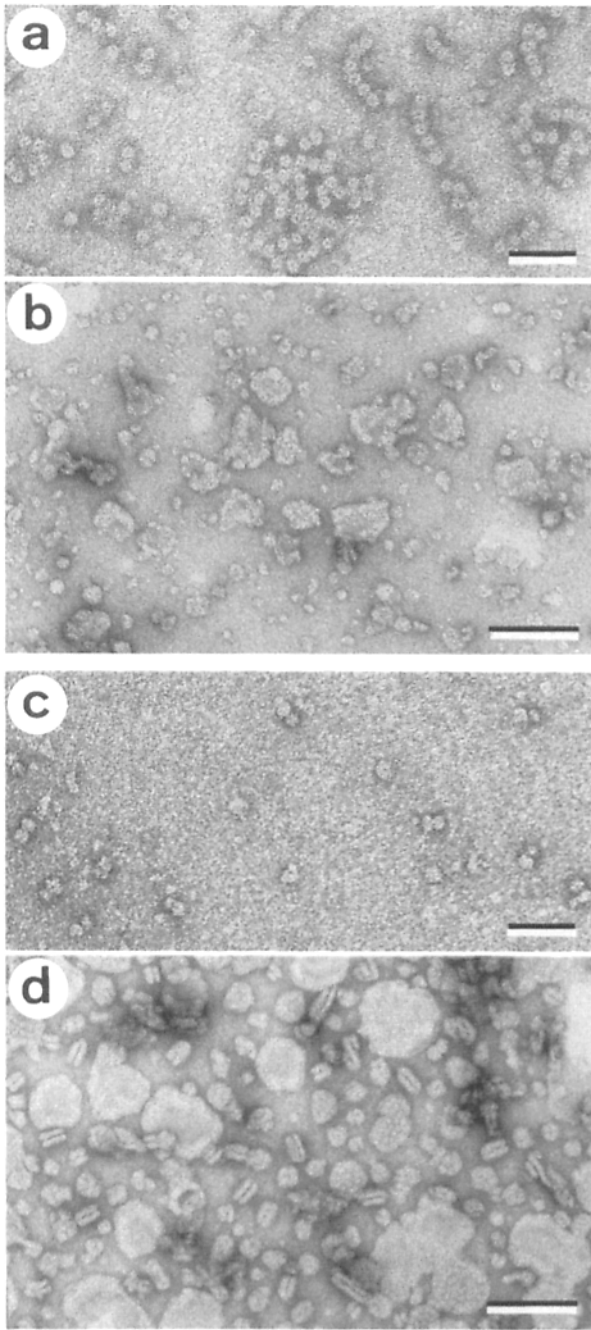
Figure 5. Crude assembly from hemichannels. (*a*) 8-POE–solubilized hemichannels appear as doughnut-shaped particles by negative stain electron microscopy. (*b*) Small membrane sheets reconstituted from 8-POE–solubilized fiber membrane proteins and lipids. Note the absence of double-layered structures. (*c*) Pairing of hemichannels by exchange of 8-POE with 10-MALT produces connexon pairs appearing as dumbbell-shaped particles. (*d*) Reconstitution of paired connexons with fiber membrane lipids yielding abundant double-layered mini gap junctions. Bars, 50 nm in *a* and *c* and 100 nm in *b* and *d*.

bine to connexon pairs before lateral assembly. These in vitro–formed connexon pairs could be visualized as a 16S peak by gradient analysis (Fig. 2 *d*) and as dumbbell-shaped structures by negative-stain electron microscopy (Fig. 5 *c*). This preparation containing paired connexons was then used

for crude assembly. In this case, mini gap junctions, as double-layered side views and as face-on views, were abundant among the reconstitution products (Fig. 5 *d*). Occasionally, clusters of channels were also found incorporated into larger membranes. This result proved our hypothesis correct that, by separating connexon pairing and lateral assembly reactions, double-layered gap junction structures could be assembled from hemichannels.

Gap junctions that were considerably larger than mini gap junctions were obtained using the gradient assembly protocol with separate steps for connexon pairing and lateral assembly. 8-POE–solubilized hemichannels were combined to connexon pairs by exchanging 8-POE with 10-MALT and then isolated as a 16S gradient peak. Addition of 10-MALT–solubilized lipids in various combinations followed by the removal of the detergent resulted in the reconstitution of large noncrystalline gap junctions (Fig. 6). The structures shown were obtained with a 1:1 mixture of DMPC and OPPC and LPR = 1. The protein concentration was maintained at 0.1 mg/ml. In many cases, the double-layered nature of these gap junctions was evident at folded edges (Fig. 6, *a* and *b*). The gap junction size was variable to a maximum size of ∼300 nm, and the larger junctions contained several hundred channels (Fig. 6 *c*). Table I lists other LPRs and lipid combinations used for reconstitution and relates them to the morphologies and approximate maximum sizes of assembled gap junctions. Channels were consistently found clustered in a noncrystalline arrangement.

The gradient assembly protocol with separate steps of connexon pairing and lateral assembly could be carried out in two different ways: in the case above, the 8-POE–soluble fraction was immediately dialyzed against 10-MALT to minimize the time span the hemichannels spent in 8-POE. The connexon pairs were then isolated as a 16S gradient peak and mixed with lipids. Alternatively, the 8-POE–soluble fraction was run on a gradient containing the same detergent, and 9S hemichannels were isolated. Connexon pairing was then accomplished by dialysis against 10-MALT, and lateral assembly promoted by reconstitution with lipids. However, in the latter procedure, protein was consistently found aggregated and adhering to amorphous membrane vesicles or sheets (Fig. 6 *d*). It appears that prolonged exposure to 8-POE rendered the channels incapable of incorporation into membranes.

STEM dark-field imaging was used to further characterize the reconstituted gap junction sheets and to resolve uncertainties concerning their layered structure. Gap junctions with folded edges were unambiguously identified as double layered. However, as was the case with the mini gap junctions, this was not possible for face-on views of the gap junction sheets. Hence, to resolve this uncertainty, STEM mass analysis was similarly applied to unstained freeze-dried gap junction sheets. The MPA for a large number of these gap junctions was determined and plotted as a histogram (not shown). The MPA peak at 9.1 ± 1.2 kD/nm² was in excellent agreement with that obtained for the mini gap junctions, showing that the gap junction sheets were generally double layered.

In summary, a novel two-step assembly procedure that starts from hemichannels produces large noncrystalline gap junctions that are indistinguishable from those formed in the lens fiber membranes in vivo.
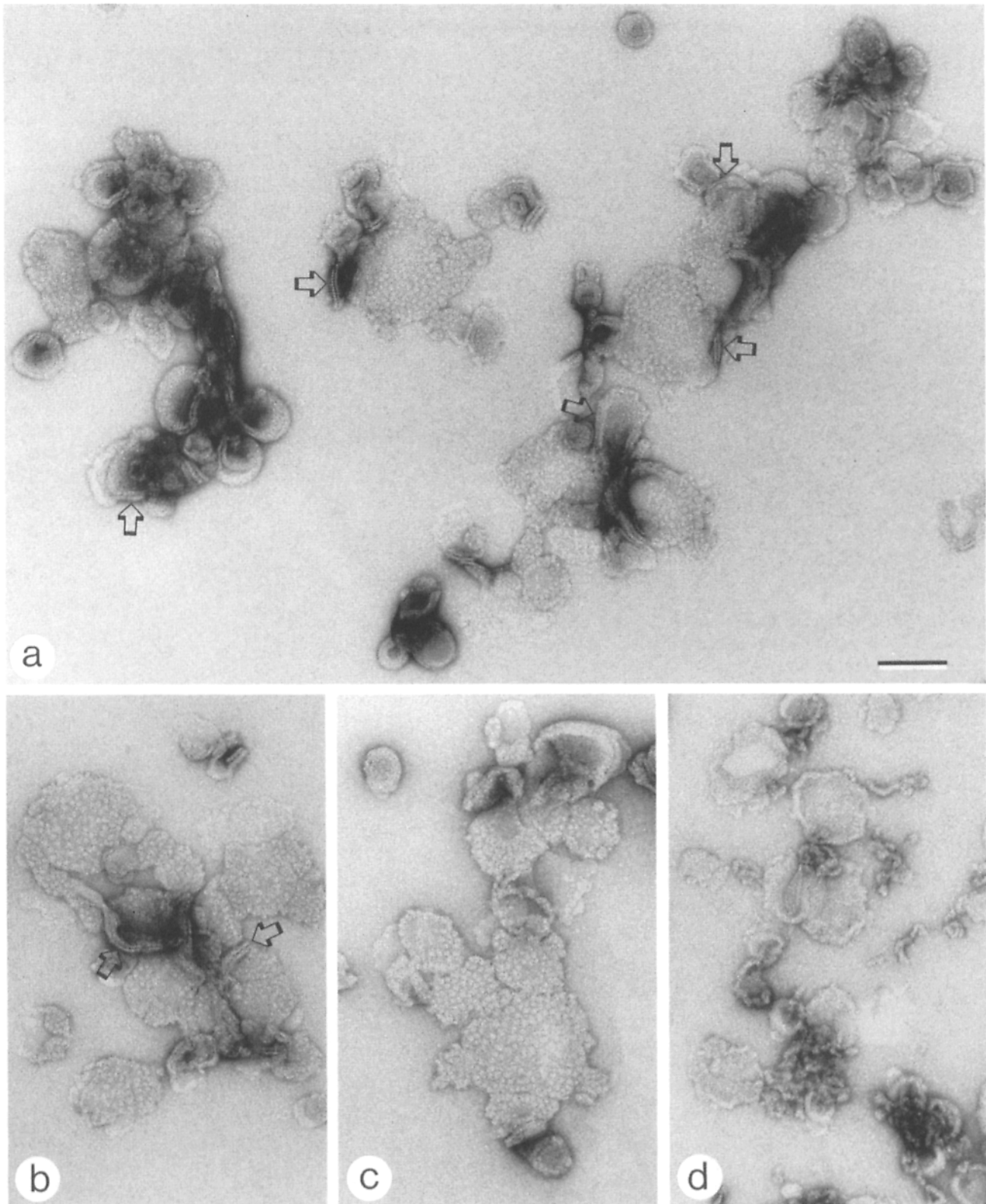
Figure 6. Gradient assembly of native-type gap junctions from hemichannels. (*a–c*) Gap junction sheets reconstituted from in vitro–paired connexons and DMPC/OPPC at LPR = 1. Channels are packed in a noncrystalline arrangement. Arrows point to folded edges where the double-layered aspect is evident. (*d*) Prolonged exposure to 8-POE renders channels incapable of membrane incorporation and results in protein aggregation. Bar, 100 nm.

Table I. Effect of Lipids on Gap Junction
Morphology and Size Using the Gradient Assembly
Procedure Starting from 9S Hemichannels

Lipids*					Gap junction assembly‡	
DMPC	OPPC	DPPE	SPH	LPR	Morphology	Maximum size
						nm
+	+	−	−	5	Integrated§	50
+	+	−	−	1	Sheets	300
+	+	−	−	0.3	Aggregated	−
+	−	−	−	1	Sheets	200
−	+	−	−	1	Sheets	100
+	+	+	−	1	Sheets	100
+	+	+	+	1	Aggregated	−
+	+	−	+	1	Aggregated	−

* Lipids were mixed in equal quantities with each other.
‡ Dialysis was at 23°C for 3 d against buffer containing 10 mM Hepes, pH
7.2, 20 mM MgCl$_2$, and 0.005% NaN$_3$.
§ Clusters of channels integrated in large membrane vesicles.

Discussion

Our strategy for the in vitro assembly of native-type non-crystalline lens fiber gap junctions has important new features that previous procedures did not have (Lampe et al., 1991; Kistler et al., 1993). These are (a) the solubilization of connexin in the form of hemichannels; (b) the separation of connexon pairing and lateral assembly into two independent reaction steps; and (c) the reconstitution with defined lipid mixtures. The flow chart in Fig. 7 shows the individual steps of the new procedure including the "quality control" checks at each step. The initial solubilization as hemichan-
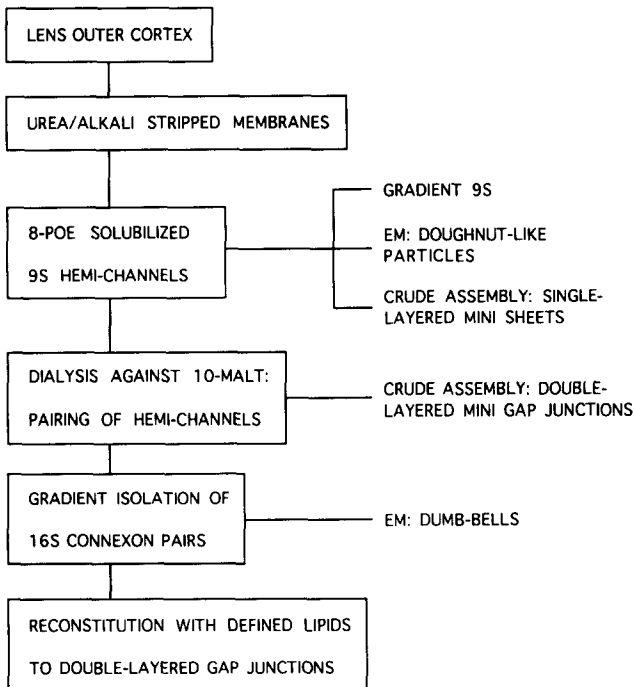

Figure 7. Flow diagram for the gradient assembly protocol that uses 8-POE-solubilized hemichannels and produces native-type non-crystalline lens fiber gap junctions. Individual steps of the procedure are listed on the left, quality control checks are on the right.

nels was verified by gradient analysis and STEM/CTEM analysis, which showed a predominant 9S peak and 388-kD doughnut-shaped structures, respectively. Crude assembly did not produce double-layered mini gap junctions because they were consistently obtained when assembly was started from connexon pairs. Formation of connexon pairs from hemichannels was verified similarly using gradient analysis and STEM/CTEM analysis, which showed a predominant 16S peak and 724-kD dumbbell-shaped structures, respectively. Crude assembly after the step of connexon pairing produced abundant double-layered mini gap junctions.

Using the in vitro–formed connexon pairs for reconstitution with defined lipid mixtures, large noncrystalline gap junctions were obtained. The type of lipids and the LPR were important (Table I). The largest gap junctions have so far been obtained using a mixture of DMPC and OPPC and LPR = 1. Surprisingly, lipid mixtures that contained DMPC, OPPC, and DPPE with or without sphingomyelin and which came closest to the lipid composition of the lens fiber membranes (Meneses et al., 1990; Fleschner and Cenedella, 1991) produced smaller gap junctions or aggregated material. It should be noted, however, that in contrast to the fiber membranes, lipid mixtures used for the in vitro reconstitution experiments did not contain cholesterol because of its poor solubility in 10-MALT.

In all cases of in vitro–assembled gap junctions, whether in the form of mini gap junctions, large gap junction sheets, or integrated into larger membranes, channels were always found clustered and never individually in the bilayer. It could be argued that major proteins such as MIP26 and MP20, which are cosolubilized in large amounts with the connexins in 8-GLU or 10-MALT (Fig. 1), compete for integration in the lipid bilayer, thereby pushing junctional channel structures together or forcing them to assemble separately as mini gap junctions. This explanation is less likely in the case of the 8-POE–solubilized material, which contained considerably smaller amounts of nonconnexin protein and which formed clusters in otherwise presumably "empty" lipid bilayers when reconstituted at LPR = 5 (Table I). The clustering of channels may be spontaneous or may depend on "helper" proteins. We cannot exclude the latter possibility because of the fact that hemichannels or connexon pairs used for the reconstitution experiments were not biochemically pure and contained various amounts of MIP26 and other minor proteins. Mg^{2+}, which was found to be a prerequisite for the formation of the large gap junction sheets, may be involved in protein–protein interactions or in the stabilization of lipid head group interactions. The irregular arrangement of channels suggests that interactions between channels are weak. The relatively loosely spaced arrangement could be explained if the long carboxy terminal tails of the lens fiber connexins (Paul et al., 1991; White et al., 1992) were in a randomized configuration around the channel, assuming that interactions between channels occurred in this carboxy-terminal portion of the molecules. Cleavage of the carboxy-terminal portion abolishes the ability of channel structures to arrange irregularly in reconstituted junctions and interactions involving different sites of the molecules must be responsible for the formation of crystalline lattices (Kistler et al., 1990a; Lampe et al., 1991). In this context, it should also be pointed out that the edge views of reconstituted lens fiber gap junctions do not display a characteristic pentalami-

nar appearance, and this may be caused by the flexibility of the large cytoplasmic tails of connexin50/46.

In our experiments, formation of connexon pairs from hemichannels must precede lateral assembly to form double-layered gap junction structures. Connexon pairing is induced solely by exchanging 8-POE with 10-MALT. This phenomenon could be interpreted in two ways: first, both detergents might bind to or near the sites of interaction, but only 8-POE and not 10-MALT binding interferes with connexon pairing. Alternatively, 8-POE might bind elsewhere on the connexin molecules, causing protein conformational changes that render the hemichannels incapable of pairing. Replacement of this detergent with 10-MALT reverts the connexins to their native state, and pairing is reinstated. Our results indicate that interactions between connexons are not ionic or based on disulfide exchange. It should be noted, however, that some variability may exist between different connexin types because DTT was required for the solubilization of gap junction channels from liver (Stauffer et al., 1991) and heart (Manjunath and Page, 1986), and disulfide exchange was shown to be important for the formation of functional channels between microinjected *Xenopus* oocyte pairs (Dahl et al., 1992).

The structural similarity between the noncrystalline gap junctions reconstituted from detergent-solubilized hemichannels and those formed in the lens fiber membranes (Kuszak et al., 1982; Zampighi et al., 1989; Lo and Reese, 1993) is so remarkable that it is tempting to speculate on similarities also of the assembly processes. Our data do not exclude the possibility that other membrane proteins are involved, but suggest strongly that gap junction assembly does not depend on the presence of cytoplasmic proteins or on energy input. It was previously shown that adhesion proteins play a role for gap junction assembly in vivo (Musil and Goodenough, 1991), and in the case of lens fiber gap junctions, we cannot exclude that MIP26 is involved in the assembly process (Gruijters, 1989). This is different from acetylcholine receptor channel complexes, where clustering is known to be driven by peripheral proteins (Froehner, 1991). We would further predict from our results that hemichannels that have been transported to the plasma membrane and into an area of membrane contact form connexon pairs between hemichannels of adjacent cells before joining a forming gap junction. This would seem important also conceptually because immobilization of hemichannels in an unordered lattice would make pairing with equally immobilized hemichannels in the opposing membrane almost impossible. It should be noted, however, that these extrapolations of our results to the situation in vivo have several limitations. For example, we have ignored the phosphorylation state of the connexin that had previously been demonstrated to be important for gap junction assembly (Musil et al., 1990; Musil and Goodenough, 1991). Further, the stoichiometry of connexin46 and connexin50 in the channel structures is unknown. We have used as markers anti-MP70 antibodies that react only with connexin50 (White et al., 1992). Last, the reconstituted gap junctions are still considerably smaller than the largest fiber gap junctions, which can have diameters of several microns and the assembly of which might involve additional factors (Gruijters et al., 1987).

The lens system is so far unique in that gap junction channels can be solubilized under mild conditions and in that

hemichannels and connexon pairs can be isolated separately. Both forms retain the ability to reassemble into gap junctions. While the aim to reconstitute native-type lens fiber gap junctions has been fulfilled, there may be other benefits of the new procedure. By varying the assembly conditions, it may become possible to assemble crystalline lattices from uncleaved channel structures that would be suitable for high resolution structural analysis (Jap et al., 1992). Difference maps of these and those previously obtained with cleaved channel structures (Lampe et al., 1991) could then reveal the position in the channel structure of the carboxy-terminal tail of the connexin molecules (Kistler et al., 1990b). Another potential benefit of our results concerns the function of the gap junction channels. We have shown that small gap junctions integrate into membrane vesicles when appropriate reconstitution conditions are used. These vesicles could be fused with planar lipid bilayers, resulting in the incorporation of intact junctional channels. This may be a way to study the electrophysiological properties of lens fiber junctional channels more efficiently and more precisely than was hitherto possible (Donaldson and Kistler, 1992). This way, the regulation of these channels could be studied under well-defined conditions.

References

Bennett, M. V. L., L. C. Barrio, T. A. Cargiello, D. C. Spray, E. Hertzberg, and J. C. Saez. 1991. Gap junctions: new tools, new answers, new questions. *Neuron.* 6:305-320.

Beyer, E. C., D. L. Paul, and D. A. Goodenough. 1987. Connexin43: a protein from rat heart homologous to a gap junction protein from liver. *J. Cell Biol.* 105:2621-2629.

Beyer, E. C., D. L. Paul, and D. A. Goodenough. 1990. Connexin family of gap junction proteins. *J. Membr. Biol.* 116:187-194.

Dahl, G., R. Werner, E. Levine, and C. Rabadandiehl. 1992. Mutational analysis of gap junction formation. *Biophys. J.* 62:172-182.

Donaldson, P., and J. Kistler. 1992. Reconstitution of channels from preparations enriched in lens gap junction protein MP70. *J. Membr. Biol.* 129: 155-165.

Engel, A., and C. Colliex. 1993. Application of scanning transmission electron microscopy to the study of biological structure. *Curr. Opin. Biotech.* 4: 403-411.

Fallon, R., and D. A. Goodenough. 1981. Five hour half life of mouse liver gap junctions. *J. Cell Biol.* 90:521-526.

Fishman, G. I., D. C. Spray, and L. A. Leinwand. 1990. Molecular characterization and functional expression of the human cardiac gap junction channel. *J. Cell Biol.* 111:589-597.

Fleschner, C. R., and R. J. Cenedella. 1991. Lipid composition of lens plasma membrane fractions enriched in fiber junctions. *J. Lipid Res.* 32:45-53.

Froehner, S. C. 1991. The submembrane machinery for nicotinic acetylcholine receptor clustering. *J. Cell Biol.* 114:1-7.

Gruijters, W. T. M., J. Kistler, and S. Bullivant. 1987. Formation, distribution, and dissociation of intercellular junctions in the lens. *J. Cell Sci.* 88: 351-359.

Gruijters, W. T. M. 1989. A non-connexon protein (MIP) is involved in eye lens gap junction formation. *J. Cell Sci.* 93:509-513.

Hertzberg, E. L. 1984. A detergent independent procedure for the isolation of gap junctions from rat liver. *J. Biol. Chem.* 259:9936-9943.

Jap, B. K., M. Zulauf, T. Scheybani, W. Baumeister, U. Aebi, and A. Engel. 1992. 2D crystallization: from art to science. *Ultramicroscopy.* 46:45-84.

Kistler, J., B. Kirkland, and S. Bullivant. 1985. Identification of a 70,000 D

protein in lens fiber junctional domains. *J. Cell Biol.* 101:28–35.

Kistler, J., D. Christie, and S. Bullivant. 1988. Homologies between gap junction proteins in lens, heart and liver. *Nature (Lond.).* 331:721–723.

Kistler, J., and S. Bullivant. 1988. Dissociation of lens fiber gap junctions releases MP70. *J. Cell Sci.* 91:415–421.

Kistler, J., J. Berriman, C. W. Evans, W. T. M. Gruijters, D. Christie, A. Corin, and S. Bullivant. 1990a. Molecular portrait of lens gap junction protein MP70. *J. Struct. Biol.* 103:204–211.

Kistler, J., J. Schaller, and H. Sigrist. 1990b. MP38 contains the membrane embedded domain of the lens fiber gap junction protein MP70. *J. Biol. Chem.* 265:13357–13361.

Kistler, J., J. Bond, P. Donaldson, and A. Engel. 1993. Two distinct levels of gap junction assembly in vitro. *J. Struct. Biol.* 110:28–38.

Kren, B. T., N. M. Kumar, S. Wang, N. B. Gilula, and C. J. Steer. 1993. Differential regulation of multiple gap junction transcripts and proteins during rat liver regeneration. *J. Cell Biol.* 123:707–718.

Kumar, N. M., and N. B. Gilula. 1986. Cloning and characterization of human and rat liver cDNAs coding for a gap junction protein. *J. Cell Biol.* 103:767–776.

Kumar, N. M., and N. B. Gilula. 1992. Molecular biology and genetics of gap junction channels. *Sem. Cell Biol.* 3:3–16.

Kuszak, J. R., J. L. Rae, B. U. Pauli, and R. S. Weinstein. 1982. Rotary replication of lens gap junctions. *J. Ultrastruct. Res.* 81:249–256.

Laemmli, U. K. 1970. Cleavage of structural proteins during the assembly of the head of bacteriophage T4. *Nature (Lond.).* 227:680–685.

Laird, D., K. Puranam, and J. P. Revel. 1991. Turnover and phosphorylation dynamics of connexin43 gap junction protein in cultured cardiac myocytes. *Biochem. J.* 273:67–72.

Lampe, P. D., J. Kistler, A. Hefti, J. Bond, S. Müller, R. G. Johnson, and A. Engel. 1991. In vitro assembly of gap junctions. *J. Struct. Biol.* 107:281–290.

Lo, W. K., and T. S. Reese. 1993. Multiple structural types of gap junctions in mouse lens. *J. Cell Sci.* 106:227–235.

Lowry, O. H., N. J. Rosenbrough, A. L. Farr, and R. J. Randall. 1951. Protein measurement with the folin phenol reagent. *J. Biol. Chem.* 193:265–275.

Manjunath, C. K., G. E. Goings, and E. Page. 1985. Proteolysis of cardiac gap junctions during their isolation from rat hearts. *J. Membr. Biol.* 85:159–168.

Manjunath, C. K., and E. Page. 1986. Rat heart gap junctions as disulfide-bonded connexon multimers: their depolymerization and solubilization in deoxycholate. *J. Membr. Biol.* 90:43–57.

Meneses, P., J. V. Greiner, and T. Glonek. 1990. Comparison of membrane phospholipids of the rabbit and pig crystalline lens. *Exp. Eye Res.* 50:235–240.

Müller, S. A., K. N. Goldie, R. Buerki, R. Haering, and A. Engel. 1992. Factors influencing the precision of quantitative scanning transmission electron microscopy. *Ultramicroscopy.* 46:317–334.

Musil, L. S., B. A. Cunningham, G. M. Edelman, and D. A. Goodenough. 1990. Differential phosphorylation of the gap junction protein connexin43 in junctional communication-competent and -deficient cell lines. *J. Cell Biol.* 11:2077–2088.

Musil, L. S., and D. A. Goodenough. 1991. Biochemical analysis of connexin43 intracellular transport, phosphorylation, and assembly into gap junctional plaques. *J. Cell Biol.* 115:1357–1374.

Musil, L. S., and D. A. Goodenough. 1993. Multisubunit assembly of an integral plasma membrane channel protein, gap junction connexin43, occurs after exit from the ER. *Cell.* 74:1065–1077.

Nicholson, B., R. Dermietzel, D. Teplow, O. Traub, K. Willecke, and J. P. Revel. 1987. Two homologous protein components of hepatic gap junctions. *Nature (Lond.).* 329:732–734.

Nishi, M., N. M. Kumar, and N. B. Gilula. 1991. Developmental regulation of gap junction gene expression during mouse embryonic development. *Dev. Biol.* 146:117–130.

Paul, D. L., and D. A. Goodenough. 1983. Preparation, characterization, and localization of antisera against bovine MIP26, an integral protein from lens fiber plasma membrane. *J. Cell Biol.* 96:625–632.

Paul, D. L. 1986. Molecular cloning of cDNA for rat liver gap junction proteins. *J. Cell Biol.* 103:123–134.

Paul, D. L., L. Ebihara, L. J. Takemoto, K. I. Swenson, and D. A. Goodenough. 1991. Connexin46, a novel lens gap junction protein, induces voltage-gated currents in non-junctional plasma membrane of Xenopus oocytes. *J. Cell Biol.* 115:1077–1089.

Revel, J. P., J. H. Hoh, S. A. John, D. W. Laird, K. Puranam, and S. B. Yancey. 1992. Aspects of gap junction structure and assembly. *Sem. Cell Biol.* 3:21–28.

Risek, B., F. G. Klier, and N. B. Gilula. 1992. Multiple gap junction genes are utilized during rat skin and hair development. *Development.* 116:639–651.

Sas, D. F., M. J. Sas, K. R. Johnson, A. S. Menko, and R. G. Johnson. 1985. Junctions between lens fiber cells are labeled with a monoclonal antibody shown to be specific for MIP26. *J. Cell Biol.* 100:216–225.

Saxton, O. W., T. J. Pitt, and M. Horner. 1979. Digital image processing: the Semper system. *Ultramicroscopy.* 4:343–354.

Stauffer, K. A., N. M. Kumar, N. B. Gilula, and N. Unwin. 1991. Isolation and purification of gap junction channels. *J. Cell Biol.* 115:141–150.

Swenson, K. I., J. R. Jordan, E. C. Beyer, and D. L. Paul. 1989. Formation of gap junctions by expression of connexins in *Xenopus* oocyte pairs. *Cell.* 57:145–155.

White, T. M., R. Bruzzone, D. A. Goodenough, and D. L. Paul. 1992. Mouse connexin50, a functional member of the connexin family of gap junction proteins, is the lens fiber protein MP70. *Mol. Biol. Cell.* 3:711–720.

Willecke, K., H. Hennemann, E. Dahl, S. Jungbluth, and R. Heynkes. 1991. The diversity of connexin genes encoding gap junctional proteins. *Eur. J. Cell Biol.* 56:1–7.

Yeager, M., and N. B. Gilula. 1992. Membrane topology and quaternary structure of cardiac gap junction ion channels. *J. Mol. Biol.* 223:929–948.

Yancey, S. B., S. Biswal, and J. P. Revel. 1992. Spatial and temporal patterns of distribution of the gap junction protein connexin43 during mouse gastrulation and organogenesis. *Development.* 144:203–212.

Zampighi, G. A., J. E. Hall, G. R. Ehring, and S. A. Simon. 1989. The structural organization and protein composition of lens fiber junctions. *J. Cell Biol.* 108:2255–2275.

Zhang, J. T., and B. J. Nicholson. 1989. Sequence and tissue distribution of a second protein of hepatic gap junctions, Cx26, as deduced from its cDNA. *J. Cell Biol.* 109:3391–3401.